Noise-covered drift bifurcation of dissipative solitons in a planar gas-discharge system

H. U. Bödeker,[1,*] M. C. Röttger,[1] A. W. Liehr,[1] T. D. Frank,[2] R. Friedrich,[2] and H.-G. Purwins[1]
[1]*Institut für Angewandte Physik, Corrensstraße 2/4, 48149 Münster, Germany*
[2]*Institut für Theoretische Physik, Wilhelm-Klemm-Straße 9, 48149 Münster, Germany*
(Received 29 December 2002; published 28 May 2003)

The trajectories of propagating self-organized, well-localized solitary patterns (*dissipative solitons*) in the form of electrical current filaments are experimentally investigated in a planar quasi-two-dimensional dc gas-discharge system with high Ohmic semiconductor barrier. Earlier phenomenological models qualitatively describing the experimental observations in terms of a particle model predict a transition from stationary filaments to filaments traveling with constant finite speed due to an appropriate change of the system parameters. This prediction motivates a search for a drift bifurcation in the experimental system, but a direct comparison of experimentally recorded trajectories with theoretical predictions is impossible due to the strong influence of noise. To solve this problem, the filament dynamics is modeled using an appropriate Langevin equation, allowing for the application of a stochastic data analysis technique to separate deterministic and stochastic parts of the dynamics. Simulations carried out with the particle model demonstrate the efficiency of the method. Applying the technique to the experimentally recorded trajectories yields good agreement with the predictions of the model equations. Finally, the predicted drift bifurcation is found using the semiconductor resistivity as control parameter. In the resulting bifurcation diagram, the square of the equilibrium velocity scales linearly with the control parameter.

DOI: 10.1103/PhysRevE.67.056220 PACS number(s): 05.45.Tp, 89.75.Fb, 05.10.Gg, 52.80.Tn

I. INTRODUCTION

Solitary structures are commonly observed in a rich variety of experiments, systems, and model equations including purely conservative systems [1,2] as well as systems with weak [3] and strong dissipation [4,5]. Due to the particlelike properties of these solitary structures, their dynamics and interactions are of considerable interest to modern science. Here we focus on well-localized solitary structures in dissipative systems, which we refer to as dissipative solitons (DSs), following Refs. [3,5]. They exist in biological systems as nerve pulses [6], in chemical systems as concentration drops of chemical reagents [7–9], in optical systems as bright spots in the transverse plane of propagating laser beams [10,11], and as current filaments in semiconductor devices [12–15] as well as in quasi-one- and -two-dimensional ac and dc gas-discharge systems with high Ohmic and dielectric barriers [5,16–21]. The modeling of these nonlinear dissipative systems often leads to reaction-diffusion equations [4,13,14,22–29], which, in the case of optical systems, contain cross-diffusion terms [10,11].

As well-localized solitary patterns were found as solutions of reaction-diffusion models, particle concepts have been derived starting from the original field equations. The first successful methods were developed in the context of inhomogeneity influenced trigger fronts [30], but similar methods have also been applied successfully to deal with the propagation and mutual interaction of DSs [26]. In this particle approach, the dynamics of the DSs is described by ordinary differential equations. A comparison of the results of this reduced dynamical description (in the following called *reduced dynamics*) with the results obtained from the underlying field equations yields good agreement if the shape of moving and stationary DSs does not differ significantly [26]. In particular, both reaction-diffusion equations and corresponding reduced dynamics predict a transition from stationary DSs to DSs traveling with constant finite velocity for an appropriate change of the system parameters [31]. These theoretical predictions give rise to the question whether this drift bifurcation can also be observed in experimental systems.

As a proper candidate for such a system, we have chosen a planar semiconductor gas-discharge system which under suitable conditions exhibits DSs in the form of well-localized current density filaments [17]. This choice is motivated by the fact that the experimental system was modeled as an electrical equivalent circuit for which two- and three-component reaction-diffusion equations have been set up [22,23,31]. These equations qualitatively take account of many pattern formation phenomena that are observed in the experimental system and can be reduced to a particle model near the drift bifurcation point [26,32].

However, a direct comparison of experimental observations to the model predictions is hardly possible as the experimentally recorded trajectories indicate a strong influence of noise in the system that the theoretical models do not take into account. Motivated by the particlelike properties of the DSs observed in the experiment, a Langevin equation is set up for the description of the experimentally recorded dynamics, using only the symmetries of the experimental system. The validity of the Langevin equation allows the application of a data-driven stochastic analysis method [33,34] which allows for the separation of the deterministic and stochastic parts of the dynamics. To verify the efficiency of the data analysis method, the technique is tested on data numerically generated from the equations of the reduced dynamics which

*Corresponding author.
Email address: boedeker@uni-muenster.de

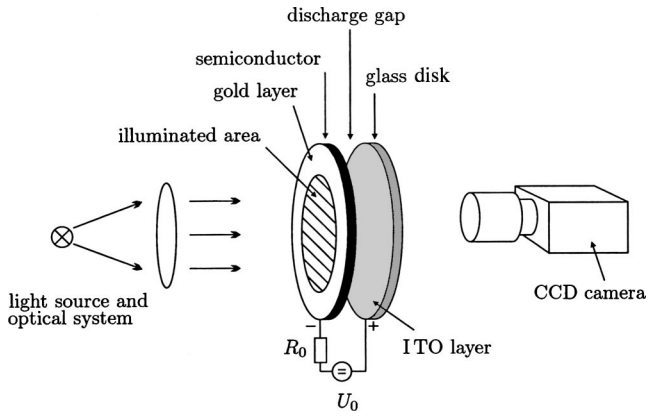

FIG. 1. Schematic representation of the experimental setup. The resistivity of the semiconductor is controlled by variable homogeneous illumination with visible light. The current distribution in the discharge gap is recorded via the luminescence radiation distribution emitted from the discharge gap.

are extended to a Langevin equation by adding appropriate noise terms. It turns out that the application of the technique with respect to the analysis of the recorded experimental data makes possible a comparison of the deterministic part of the experimentally observed dynamics of DSs to the predictions of the model equations. In this way we prove that the reduced dynamics is suitable to describe the deterministic part of the dynamics of DSs in the experimental system, and that a drift bifurcation of these DSs can take place.

The article is organized as follows. Section II describes the experimental system, the applied recording techniques, and the experimentally observed filament trajectories. In Sec. III we recall some aspects of the modeling of the experimental system by reaction-diffusion equations and describe the results of the reduction of these equations to ordinary differential equations in a particle approach. Section IV presents the stochastic data analysis technique and its adaptation to the investigated system as well as a reliability test of the method based on numerically generated data. Section V deals with the results of the application of the technique to the experimental data. Furthermore, the experimentally detected drift bifurcation is presented in this section. The article closes with a summary and an outlook in Sec. VI.

II. THE EXPERIMENT

A. Experimental setup

The experimental system is a version of an electronic device initially designed for the high speed conversion of infrared images to the visible [18,35]. Figure 1 shows the basic experimental setup, consisting of a high Ohmic semiconductor cathode contacted from one side by a semitransparent gold layer, a gas gap, and an anode consisting of a glass disk coated with a layer of indium tin oxide (ITO), which is transparent for visible light. The semiconductor is a chromium-doped gallium arsenide wafer cooled to 100 K. At this temperature the semiconductor exhibits a linear current-voltage characteristic and a high specific resistivity of $\rho_{SC} \approx 10^5$–$10^9\ \Omega\,\mathrm{cm}$, which can be controlled via the internal photo effect by illumination. The gas in which the discharge takes place is pure nitrogen at a pressure of $p \approx 300$ hPa. While the current-voltage characteristic of the wafer is linear, the current-voltage characteristic of the gas is highly nonlinear and partly exhibits negative differential resistivity. The maximum global current of the system is restricted by a series resistor R_0 of some MΩ. Since the electrical current density in the discharge plane of the described device and the density of the luminescence radiation emitted from the discharge space locally are proportional to each other over a large range, the current density distribution can be measured via the luminescence density distribution through the transparent anode (see Fig. 1). To record the corresponding images, a charge-coupled device (CCD) camera with video frequency was used.

B. Experimental observations

For certain parameters of the gas-discharge system, self-organized spatially inhomogeneous luminescence density patterns are observed in the discharge gap. Among other things, we also observe well-localized bright solitary spots in the luminescence radiation distribution that are related to self-organized current filaments. These filaments may travel or stay at rest. In addition, they can interact, and scattering, formation of molecules, and generation and annihilation are frequently observed phenomena [17,36]. To obtain filament trajectories from the recorded data, first the filaments of each recorded image are identified using a recursive algorithm searching for connected regions of high luminance. In the second step, the ''center of mass'' of each filament is determined. Finally, a trajectory of each filament is generated using a nearest neighbor tracing algorithm. In the present paper, the system parameters are always chosen such that only one filament exists at a given time. In this way, the possible interaction of filaments is excluded.

While performing the experiment, great care is taken to assure spatial homogeneity of the system since inhomogeneities may affect the filament dynamics. The homogeneity was controlled in two ways. First, the device was operated in a mode where no spatial patterns occur. Under these conditions, no indications of possible inhomogeneities in the luminescence distribution were observed. Second, trajectories of moving filaments were analyzed with respect to their statistical behavior. The fact that the relevant statistical characteristics for different trajectories that in general probe different areas of the discharge plane show no significant deviations also strongly supports the hypothesis that the system is rather homogeneously prepared.

Figures 2(a) and 2(b) show trajectories of filaments obtained in the described way for two different sets of system parameters. The circle indicates the border of the area of the gas-discharge plane defined by the mechanical spacer used. Clearly, this boundary has no measurable influence on the dynamics of the DSs since they tend to be located in an internal circle of diameter 15 mm in the center of the discharge area. This confinement in the ''active discharge area'' is caused by homogeneously illuminating the high Ohmic

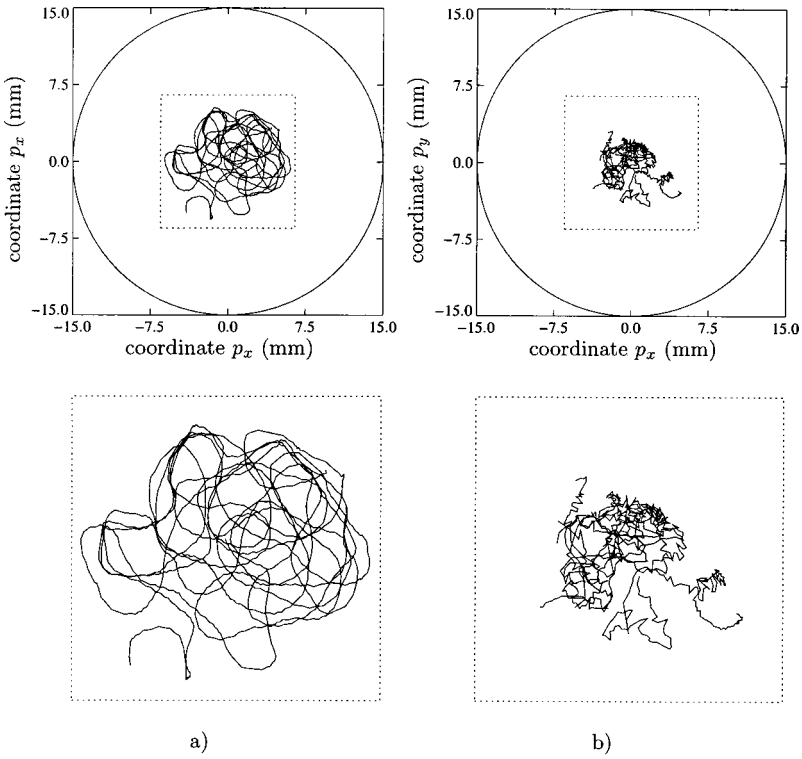

FIG. 2. Experimentally recorded trajectories of moving DSs. The circle of diameter $D=30$ mm indicates the boundary of the area of the gas-discharge plane defined by the mechanical spacer. The active discharge area is slightly larger than the space filled with trajectories. (a) Parameters: global voltage $U_0=2740$ V, semiconductor resistivity $\rho_{SC}=4.95\times10^7$ Ω cm, series resistance $R_0=20$ MΩ, pressure $p=280$ hPa, temperature of semiconductor $T_{SC}=105$ K, thickness of semiconductor $a_{SC}=1$ mm, discharge gap width $d=250$ μm, exposure time $t_{exp}=0.02$ s, recording frequency $f_{rep}=50$ Hz, observed global current $I=46$ μA. (b) Parameters: $U_0=3600$ V, $\rho_{SC}=2.02\times10^6$ Ω cm, $R_0=10$ MΩ, $p=282$ hPa, $d=550$ μm, all other parameters as in (a), observed global current $I=116$ μA.

semiconductor electrode, generating a circular shaped area of defined specific resistivity.

Both trajectories indicate a strong influence of noise in the system as the direction of motion changes inside the active area in spite of the homogeneous preparation of the system. The fluctuations might be related to noise in the semiconductor (generation and recombination, $1/f$ noise), thermal fluctuations in the gas, or noisy processes of charge transportation through the semiconductor-gas interface [37]. However, a comparison of Figs. 2(a) and 2(b) shows that in (a) the trajectories are somewhat smoother than in (b). This is reflected by the fact that the direction of motion in (b) changes significantly more frequently than in (a). Since from theoretical considerations one may expect a nontrivial deterministic part to the dynamics of the DSs, the difference of the behavior of the trajectories of (a) with respect to (b) may be attributed to a difference in this part of the dynamics.

III. A QUALITATIVE MODEL FOR THE EXPERIMENTAL SYSTEM

A. The three-component reaction-diffusion model

To interpret the pattern formation in the experimental device, we recall that for such systems a phenomenological two-component and a three-component qualitative activator-inhibitor reaction-diffusion model have been proposed on the basis of an electric equivalent circuit [23,31,38–40]. In these models, the activating component is related to the avalanche multiplication of charge carriers in the discharge gap, while the voltage drop at the semiconductor wafer takes the role of one inhibitor. The two-component version of the reaction-diffusion model permits a qualitative understanding of the formation of many stationary patterns, e.g., Turing structures [29,41–45] and stationary DSs [5,22,38,23,44] and their bound states [32] in planar dc gas-discharge systems. Similar models have also been investigated in various other fields [27–29]. In particular, we mention the work [46,47], in which the authors investigated moving DSs in more than one spatial dimension, showing that a single moving DS can be stabilized using a global feedback term. However, as discussed in Refs. [26,40], the global feedback term is not sufficient to stabilize two distinct DSs. It has also been shown analytically that a moving two-dimensional DS exists, in principle, in a delicate limit case of the standard FitzHugh-Nagumo model [48]. However, this result has not been confirmed by numerical simulations. The difficulty of describing the motion of more than one DS in two- and three-dimensional space can easily be overcome by introducing a second inhibiting component phenomenologically, so that the description of multiple stable moving DSs becomes possible without a change of the fundamental dynamical principles [26,31,40,49]. In the context of planar dc gas-discharge systems, the second inhibitor component might be related to the voltage drop in the gas region close to one of the electrodes [50] or to the influence of surface charges at the semiconductor-gas interface. Therefore, in the present analysis we apply the following three-component reaction-diffusion system:

$$\begin{aligned} \dot{u} &= D_u \Delta u + \lambda u - u^3 - \kappa_3 v - \kappa_4 w + \kappa_1, \\ \tau \dot{v} &= D_v \Delta v + u - v, \\ \theta \dot{w} &= D_w \Delta w + u - w. \end{aligned} \tag{1}$$

Here, $u(\boldsymbol{r},t)$, $v(\boldsymbol{r},t)$, and $w(\boldsymbol{r},t)$ are elements of $C^2(\Omega \times \mathbb{R})$, where Ω is a finite subset of $\mathbb{R}^2$, and D_u, D_v, D_w, λ, τ, θ, κ_1, κ_3, and κ_4 are real constants, which are positive except for κ_1. In the parameter limit $D_v \to 0$ and $\theta \to 0$, the system (1) reduces to a two-component reaction-diffusion system with local feedback term due to the fast inhibitor w. For this parameter limit and concerning stationary DSs, the shape of the slow inhibitor v is identical with the shape of the activator u, and it can be proved [26,31] that a drift bifurcation from stationary to moving DSs occurs if the time constant τ of the slow inhibitor v is increased above the critical threshold $\tau_c = 1/\kappa_3$.

The weak point of the model of Eqs. (1) is, first of all, that it is not possible to identify the component w in the experimental system in an unambiguous way. The same problem exists for some of the parameters. We also remark that the experimental setup contains a series resistor R_0 (see Fig. 1) that should lead to global inhibition via an integral term in the first line of Eqs. (1). However, this term has been eliminated to simplify numerical calculations:

$$\kappa_1' - \frac{\kappa_2}{\|\Omega\|} \int_\Omega u \, \mathrm{d}\Omega \to \kappa_1 = \text{const} \tag{2}$$

if the integral term is approximately constant. In contrast to the mentioned drawbacks of Eqs. (1) to describe the pattern formation in the experimental gas-discharge system, the amazing fact is that a large variety of phenomena observed in the experimental system can also be found in the behavior of the solutions of Eqs. (1). Among these phenomena we find the formation of various patterns like periodic stripes, hexagonal arrangements, spirals, target patterns, and DSs. For the last, phenomena like generation, annihilation, scattering, formation of molecules, etc., are observed both in the experiment and in the mathematical equations. Also, the Turing bifurcation and the subcritical nature of bifurcations to increasing numbers of DSs can be observed in the experiment and the model equations. Some of the phenomena were predicted from the model of Eqs. (1) and were later found in the experiment, while other phenomena were first detected experimentally and could later be identified in Eqs. (1). From these qualitative successes of the model, we draw the conclusion that strong ties exist between Eqs. (1) and more specific model equations for the experimental system based on the momentum development of the Boltzmann equation, e.g., in the form of a drift-diffusion approximation similar to the set of equations applied to describe pattern formation in planar ac gas-discharge systems [51]. From these considerations we reason that using Eqs. (1) for a qualitative description of patterns and their bifurcations in dc gas-discharge systems with high Ohmic barriers has some justification.

B. The reduced dynamical system

Close to the point of the drift bifurcation, the dynamics of DSs as solutions of the field equations (1) can be reduced to ordinary differential equations by projecting the system onto its relevant modes. The drift of the DS in the described parameter limit is induced by the so-called *propagator mode*, which corresponds to the displacement between the activator and the slow inhibitor distribution of the individual DS [26,30]. In the reduced system, the direction of motion and the velocity of the movement are given by the amplitude of propagator mode $\boldsymbol{\alpha} = \boldsymbol{\alpha}(t)$ which, for a single soliton, is connected to the position $\boldsymbol{p} = \boldsymbol{p}(t)$ of the DS by the following relations (called the reduced dynamics):

$$\dot{\boldsymbol{p}} = \kappa_3 \boldsymbol{\alpha}, \tag{3}$$

$$\dot{\boldsymbol{\alpha}} = \kappa_3^2 \left(\tau - \frac{1}{\kappa_3} \right) \boldsymbol{\alpha} - \kappa_3 \underbrace{\frac{\langle \bar{u}_{xx}^2 \rangle}{\langle \bar{u}_x^2 \rangle}}_{=:Q} |\boldsymbol{\alpha}|^2 \boldsymbol{\alpha}. \tag{4}$$

The angular brackets denote averaging over the whole domain. The shape factor Q can be computed from the activator distribution $\bar{u}$ of a stationary DS solution for a given set of system parameters. If several DSs are interacting, Eqs. (3) and (4) have to be solved for every DS, and each equation must be supplemented by an interaction term $F(|\boldsymbol{p}_i - \boldsymbol{p}_j|)(\boldsymbol{p}_i - \boldsymbol{p}_j)$ for each interacting pair of DSs at positions $\boldsymbol{p}_i$ and $\boldsymbol{p}_j$. This interaction term depends on the distance between the interacting DSs and, like the shape factor Q, can be computed from a stationary DS solution.

From Eq. (3) it can be seen that for a single noninteracting DS, the amplitude of the propagator mode $\boldsymbol{\alpha}$ is proportional to the velocity $\dot{\boldsymbol{p}}$. In addition, Eq. (4) shows that for $\tau \leqslant 1/\kappa_3$ only stationary solutions with $|\dot{\boldsymbol{p}}| = 0$ exist, whereas for $\tau > 1/\kappa_3$ this solution becomes unstable and a stable solution moving with the intrinsic velocity

$$|\dot{\boldsymbol{p}}| = v_0 = \kappa_3^{3/2} \sqrt{\frac{\tau - 1/\kappa_3}{Q}} \tag{5}$$

appears [26,31]. A comparison of this result with solutions of the field equations (1) in two- and three-dimensional systems shows good agreement [31,49]. We note that the reduced dynamics of a single DS [Eqs. (3) and (4)] can be written in terms of a single ordinary differential equation of second order as

$$\ddot{\boldsymbol{p}} = \kappa_3 (\kappa_3 \tau - 1) \dot{\boldsymbol{p}} - \frac{Q}{\kappa_3} |\dot{\boldsymbol{p}}|^2 \dot{\boldsymbol{p}}, \tag{6}$$

formally describing the dynamics of a unit mass particle that can undergo a bifurcation from a stationary state to a moving state with dynamically stabilized intrinsic velocity when the "friction" $\kappa_3(\kappa_3\tau - 1)$ changes sign. The nature of this bifurcation corresponds to the normal form of a drift bifurcation, which is commonly observed in synergetic systems with continuous symmetries [30,52–54].

In contrast to the deterministic dynamics described by Eqs. (1), (3), and (4), we observe that in the experiment the dynamics of DSs is strongly influenced by stochastic fluctuations, which make a direct comparison of the experimental findings with predictions of the above equations impossible. Therefore we choose for the description of the experimental recordings an appropriate stochastic ansatz as a basis for a data analysis technique discussed in the next section. The

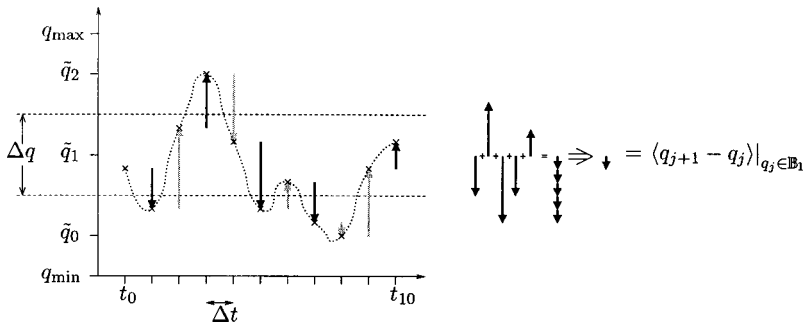

FIG. 3. Illustration of the stochastic data analysis in one dimension. A short trajectory $q(t)$ with superimposed deterministic and stochastic dynamics is shown. The trajectory is known at discrete points of time t_j and therefore represents a time series $q_j = q(t_j)$. The difference $\Delta q_j = (q_{j+1} - q_j)$ of each q_j from its successor q_{j+1} is visualized by a vector of appropriate length. In order to determine the deterministic part of the dynamics, the interval $[q_{min}, q_{max}]$ is divided into three bins $\mathbb{B}_i$, $i = 1,2,3$, with center $\tilde{q}_i$ and of width Δq. In this diagram the averaging algorithm is visualized for bin $\mathbb{B}_1$, where all differences Δq_j with $q_j \in \mathbb{B}_1$ (dark vectors) are summed up and divided by their number $N_1 = 5$. The result is the approximated deterministic part of the dynamics at $\tilde{q}_1$ multiplied by the time interval Δt.

goal of this is to make available a method that permits separation of the deterministic and stochastic part of the dynamics of the experimentally observed DSs, allowing a comparison with the model equations.

IV. STOCHASTIC DATA ANALYSIS

A. General introduction to stochastic data analysis

A wide and important class of stochastic dynamical systems are the continuous Markovian systems in n dimensions which are governed by the Langevin equation

$$\frac{d}{dt} q_i(t) = h_i(\{q_k(t)\},t) + g_{ij}(\{q_k(t)\},t)\Gamma_j(t), \quad i = 1, \ldots, n, \tag{7}$$

consisting of a deterministic and a stochastic part for a set of n stochastic variables $\{q_k(t)\}$, $k = 1, \ldots, n$. The function $\boldsymbol{h}$ describes the deterministic drift whereas the stochastic part is expressed by the second term, which is a product of the matrix of noise amplitudes $\underline{\boldsymbol{g}}(\boldsymbol{q},t) = \{g_{ij}(\boldsymbol{q},t)\}$ and a vector $\boldsymbol{\Gamma}$ of n fluctuating Langevin forces. These forces are usually assumed to be δ-correlated Gaussian-distributed noise forces with vanishing mean:

$$\langle \Gamma_i(t) \rangle = 0, \quad i = 1, \ldots, n, \tag{8}$$

$$\langle \Gamma_i(t)\Gamma_j(t') \rangle = 2\,\delta_{ij}\delta(t - t'), \quad i,j = 1, \ldots, n. \tag{9}$$

Here, the angular brackets denote the ensemble average. Equation (9) characterizes the fluctuations as white noise. Under these conditions, the following relations have been proved in a strict mathematical way [55,56], using Stratonovich's definition for stochastic integrals [57]:

$$h_i(\boldsymbol{q}) + g_{kj}(\boldsymbol{q}) \frac{\partial}{\partial q_k} g_{ij}(\boldsymbol{q}) = \lim_{\Delta t \to 0} \frac{1}{\Delta t} \langle q_i'(t + \Delta t) - q_i'(t) \rangle|_{\boldsymbol{q}'(t) = \boldsymbol{q}}, \tag{10}$$

$$g_{ik}(\boldsymbol{q}) g_{jk}(\boldsymbol{q}) = \frac{1}{2} \lim_{\Delta t \to 0} \frac{1}{\Delta t} \langle [q_i'(t + \Delta t) - q_i'(t)][q_j'(t + \Delta t) - q_j'(t)]^T \rangle|_{\boldsymbol{q}'(t) = \boldsymbol{q}}, \tag{11}$$

if $\boldsymbol{q}'(t)$ is a solution of Eq. (7). For the practical data analysis it is assumed that Eqs. (10) and (11) stay approximately valid for finite Δt, if Δt is smaller than the characteristic time scale of the system dynamics [33,34]. Here the ensemble average is replaced by the average over all times $t = t_i$ of the time series for which $\boldsymbol{q}'(t_i) \approx \boldsymbol{q}$ with $t_i = t_0 + i\Delta t$. An illustrative example of this noise filtering technique for the one-dimensional case is given in the following subsection.

B. Illustration of the stochastic data analysis technique

To illustrate the technique presented in the last section, a simple example has been considered. Figure 3 shows the one-dimensional trajectory of a dynamic variable $q(t) \in [\min_t q(t), \max_t q(t)] = [q_{min}, q_{max}] \subset \mathbb{R}$. A stroboscopic view onto the trajectory at equally spaced points of time $t_j = t_0 + j\Delta t$, $j = 0, \ldots, 10$ yields a time series $q_j := q(t_j)$. A discretization is chosen such that the interval $[q_{min}, q_{max}]$ is divided into three nonoverlapping subsets $\mathbb{B}_i = [\tilde{q}_i - \Delta q/2, \tilde{q}_i + \Delta q/2[$ for $i = 0,1$ and $\mathbb{B}_2 = [\tilde{q}_2 - \Delta q/2, \tilde{q}_2 + \Delta q/2]$, with equal width Δq and center $\tilde{q}_i$. In the following these subsets $\mathbb{B}_i$ are called *bins*.

The analysis algorithm now works as follows. Each bin $\mathbb{B}_i$ is assigned a scalar $\hat{q}_i = 0$ and a counter $N_i = 0$. The algorithm assigns each element q_j of the time series to its corresponding bin $\mathbb{B}_i$ (i.e., $q_j \in \mathbb{B}_i$), increases the counter N_i by 1, and adds $(q_{j+1} - q_j)$ to $\hat{q}_i$. After all elements q_j of the time series have been assigned to a bin, the deterministic part of the dynamics is computed by dividing the value $\hat{q}_i$ of each bin $\mathbb{B}_i$ by its counting rate N_i and the time discretization Δt.

This algorithm is visualized in Fig. 3, where for each element of the time series q_j the difference $(q_{j+1} - q_j)$ is symbolized by a vector of appropriate length. The vectors starting in bin $\mathbb{B}_1$ are marked black, whereas all other vectors

are shown in gray. In accordance with the averaging algorithm discussed, all black vectors are assigned to bin $\mathbb{B}_1$, added, and divided by their number N_1. If the noise amplitude is independent of q [derivatives drop out of Eq. (10)], the deterministic part of the dynamics in $\tilde{q}_1$ is approximately given by

$$h(\tilde{q}_1) \approx \frac{\langle q_{j+1} - q_j \rangle|_{q_j \in \mathbb{B}_1}}{\Delta t}, \tag{12}$$

if the corresponding counting rate N_1 is high enough and the time discretization Δt is small compared to the time scale of the deterministic dynamics.

C. Adaptation to the experimental system

In a classical particle approach for a conservative system one would assume that the dynamical variables for the motion of a single particle are the two-dimensional spatial coordinates of its center of mass, denoted by $\boldsymbol{p}(t) = (p_x(t), p_y(t))^T$. In such a system, the dynamics can be described by an equation of the form

$$\ddot{\boldsymbol{p}}(t) = \boldsymbol{f}(\boldsymbol{p}(t)). \tag{13}$$

As the gas-discharge system is highly dissipative, additional terms for fluctuation and friction have to be added:

$$\ddot{\boldsymbol{p}}(t) = \boldsymbol{f}(\boldsymbol{p}(t)) + \boldsymbol{h}(\boldsymbol{p}(t), \dot{\boldsymbol{p}}(t)) + \underline{\boldsymbol{R}}(\boldsymbol{p}(t), \dot{\boldsymbol{p}}(t)) \boldsymbol{\Gamma}(\boldsymbol{p}(t), t). \tag{14}$$

Here $\boldsymbol{h}$ describes acceleration due to friction and internal degrees of freedom, whereas $\underline{\boldsymbol{R}}\boldsymbol{\Gamma}$ includes all forms of fluctuation as $\underline{\boldsymbol{R}}$ represents the matrix of noise amplitudes. In the following, $\dot{\boldsymbol{p}}$ will be denoted by $\boldsymbol{v} = (v_x(t), v_y(t))^T$. The homogeneous preparation of the discharge area and other measures provide translational and rotational invariance; therefore $\boldsymbol{h}$, $\underline{\boldsymbol{R}}$, and $\boldsymbol{\Gamma}$ do not depend on $\boldsymbol{p}$, and $\boldsymbol{f} \equiv \boldsymbol{0}$. This yields the equation

$$\dot{\boldsymbol{v}} = \boldsymbol{h}(\boldsymbol{v}) + \underline{\boldsymbol{R}}(\boldsymbol{v}(t)) \boldsymbol{\Gamma}(t). \tag{15}$$

In order to apply the analysis technique described above, Eqs. (8) and (9) have to be satisfied. Equation (8) can always be satisfied by introducing an offset in $\boldsymbol{h}$. Equation (9) is approximately satisfied as long as the correlation of the noise of the systems decays on a smaller time scale than the characteristic time scale of the dynamics investigated.

An experimental determination of $\underline{\boldsymbol{R}}$ by applying Eq. (11) to the two-dimensional experimental system described by Eq. (15) yields velocity independent fluctuations, i.e., $\underline{\boldsymbol{R}}(\boldsymbol{v}) = R = \text{const}$. This allows a determination of the deterministic part of the experimentally observed dynamics using Eq. (10), showing that $\boldsymbol{h}$ features radial symmetry with respect to $\boldsymbol{v}$. This symmetry can also be derived from the O(2) symmetry of the system if the finite size of the system is neglected. Introducing $\boldsymbol{h}(\boldsymbol{v}) = h_v(v) \boldsymbol{e}_{\boldsymbol{v}}$ with $v = |\boldsymbol{v}|$ and $\boldsymbol{e}_{\boldsymbol{v}} = \boldsymbol{v}/v$, Eq. (15) can therefore be rewritten as

$$\dot{\boldsymbol{v}} = h_v(v) \boldsymbol{e}_{\boldsymbol{v}} + R \boldsymbol{\Gamma}(t). \tag{16}$$

Unfortunately, the number of experimentally available data points for the described analysis is limited, resulting in a rather unsatisfying resolution of the calculated deterministic part $\boldsymbol{h}(\boldsymbol{v})$. This problem can be overcome by taking into consideration the radial symmetry of $\boldsymbol{h}(\boldsymbol{v})$, which allows a reduction of the degrees of freedom by one dimension, resulting in much better statistics and therefore providing a major step toward the analysis of experimentally detected trajectories of particles in the original two-dimensional system. According to the rotational symmetry one may rewrite Eq. (16) in polar coordinates, introducing $\boldsymbol{v} = (v \cos\varphi, v \sin\varphi)^T$ and $\boldsymbol{\Gamma} = (\Gamma_x, \Gamma_y)^{\mathrm{T}}$:

$$\begin{pmatrix} \dot{v} \\ \dot{\varphi} \end{pmatrix} = \begin{pmatrix} h_v(v) \\ 0 \end{pmatrix} + \begin{pmatrix} R\cos\varphi & R\sin\varphi \\ -\dfrac{R}{v}\sin\varphi & \dfrac{R}{v}\cos\varphi \end{pmatrix} \begin{pmatrix} \Gamma_x \\ \Gamma_y \end{pmatrix}. \tag{17}$$

Note that Eq. (17) is interpreted according to the Stratonovich calculus. It can be proved (see the Appendix) that

$$h_v(v) + \frac{R^2(v)}{v} \approx \frac{1}{\Delta t} \langle v'(t + \Delta t) - v'(t) \rangle|_{v'(t) \approx v} \tag{18}$$

if $v'(t)$ is a solution of Eq. (17). Alternatively, $h_v(v)$ can be calculated directly from $v'(t)$ by applying the following projection (for proof see the Appendix):

$$h_v(v) \approx \frac{1}{\Delta t} \left\langle \frac{[\boldsymbol{v}'(t + \Delta t) - \boldsymbol{v}'(t)] \cdot \boldsymbol{v}'(t)}{v'(t)} \right\rangle \Bigg|_{v'(t) \approx v}. \tag{19}$$

In Eqs. (18) and (19), the bins introduced in the one-dimensional example take the form of circular rings around the origin. Compared with the two-dimensional averaging process, the counting rate in each bin is greatly increased, increasing the reliability of the calculated results.

D. Efficiency test of the analysis technique on numerically generated data

Although the validity of Eqs. (18) and (19) can be proved in an exact mathematical way (see the Appendix), no exact information is given on the effectiveness of the technique when using a finite number of input data points. In order to guarantee the efficiency of the technique, suitable Langevin equations should be solved numerically and the solutions should be analyzed with the technique (19) discussed above. The result $h_v(v)$ of this analysis can then be compared with the known deterministic term of the numerically solved Langevin equation, providing an appropriate test for the data analysis technique.

As a promising candidate for this comparison, the reduced dynamics (6) of a single DS in the three-component reaction-diffusion system (1) have been chosen. It can be seen that Eq. (6) can easily be extended to a Langevin equation by adding a noise term satisfying Eqs. (8) and (9):

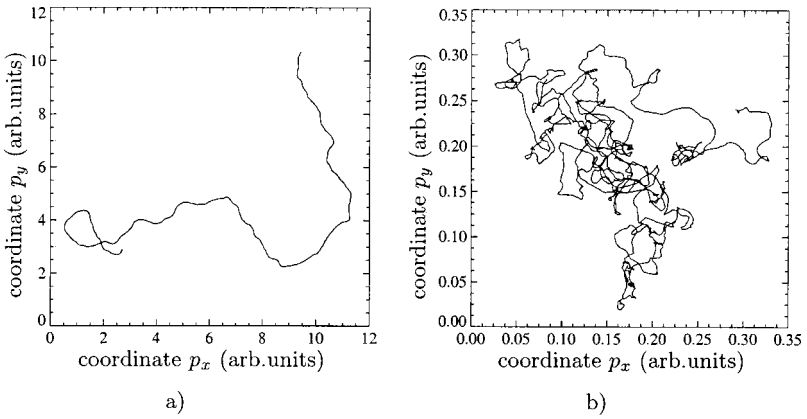

FIG. 4. Numerically calculated trajectories as a solution of the noise-extended reduced dynamics (20). (a) Trajectory of a DS above the drift bifurcation point ($\tau=3.8>\tau_c=3.\overline{3}$). Parameters: $\kappa_3=0.3$, $\Delta t=0.05$, $R=3\times10^{-4}\kappa_3$, $Q=1950$, 200 000 time steps. (b) Trajectory of a DS below the drift bifurcation point ($\tau=2.87<\tau_c=3.\overline{3}$). All other parameters are as in (a).

$$\ddot{\boldsymbol{p}}=\kappa_3(\kappa_3\tau-1)\dot{\boldsymbol{p}}-\frac{Q}{\kappa_3}|\dot{\boldsymbol{p}}|^2\dot{\boldsymbol{p}}+R\boldsymbol{\Gamma}. \tag{20}$$

This equation features rotational symmetry (16) with respect to $\dot{\boldsymbol{p}}=\boldsymbol{v}$, allowing the application of Eq. (19). For the numerical simulation, the following recursive algorithm has been used [56]:

$$\boldsymbol{v}_{n+1}=\boldsymbol{v}_n+\Delta t\left(\kappa_3(\kappa_3\tau-1)\boldsymbol{v}_n-\frac{Q}{\kappa_3}v_n^2\boldsymbol{v}_n\right)+R\sqrt{\Delta t}\boldsymbol{w}_n. \tag{21}$$

Here Δt is the time step width and $\boldsymbol{w}_n=(w_{n,x},w_{n,y})^{\mathrm{T}}$ is a vector of Gaussian-distributed random numbers satisfying $\langle w_{n,i}\rangle=0$ and $\langle w_{n,i}w_{n',j}\rangle=2\delta_{ij}\delta_{nn'}$, with $i,j=x,y$. The random numbers are generated from an equidistributed (pseudo)random number r_ν with $0\leqslant r_\nu<1$ and $\langle r_\nu\rangle=\frac{1}{2}$ via [56]

$$w_{n,i}=\sqrt{\frac{24}{M}}\sum_{\nu=1}^{M}\left(r_\nu-\frac{1}{2}\right), \tag{22}$$

where M is a large integer (in the simulation, $M=20$ has been used). As a starting point for the simulation of the noise influenced DS dynamics according to Eq. (20), the following set of parameters of the three-component reaction-diffusion system (1) was chosen, as introduced in the context of molecule formation processes [26,58]:

$$D_u=1.1\times10^{-4},\quad D_v=0,\quad D_w=9.64\times10^{-4},$$

$$\lambda=1.01,\ \kappa_1=-0.1,\quad \kappa_3=0.3,\quad \kappa_4=1,\quad \theta=0. \tag{23}$$

These parameters provide stable DS solutions in the three-component reaction-diffusion system and yield for the reduced dynamics a shape factor of $Q=1950$. The reduced dynamics predicts for this choice of parameters a supercritical bifurcation from stationary to moving DSs at the bifurcation point $\tau_c=3.\overline{3}$.

Figure 4 shows the numerically calculated trajectory of (a) an intrinsically moving DS ($\tau=3.8>\tau_c$) and (b) a stationary DS ($\tau=2.87<\tau_c$) under the influence of noise with a factor $R=3\times10^{-4}\kappa_3$. Note the striking qualitative similarities of the numerically generated and experimentally recorded trajectories (Fig. 2).

In order to test the discussed data analysis technique, we took the trajectory of the numerically calculated examples as raw data, calculated the velocities from the spatial coordinates in lowest order, and analyzed the dynamics with the discussed technique. The result is depicted in Figs. 5(a) and 6(a), where the crosses represent the deterministic part of the acceleration as a function of the particle velocity calculated using Eq. (19), and the dotted curve represents the frequency polygon of the counting rate N_i of the corresponding bins. As in every statistic analysis, the reliability of the result increases with the counting rate. As a rule of thumb, the counting rate of the bins must at least take a value between 10 and 20 to consider the corresponding result as reliable.[1]

It can be seen that as long as the counting rate is high enough, the result of the data analysis technique approximates quite well the gray curve representing the theoretical deterministic part of the dynamics (20) used to calculate the raw data for the time series. The intersection points of the theoretical curve with the abscissa mark the intrinsic velocity v_0 of the DS for the chosen system parameters. This velocity can be determined very well by the data analysis technique. Therefore we conclude that the data analysis technique is reliable and can be used for the analysis of experimentally observed two-dimensional trajectories of noninteracting DSs.

V. APPLICATION OF THE STOCHASTIC DATA ANALYSIS TO THE EXPERIMENT

A. The deterministic dynamics of experimentally observed dissipative solitons

Due to the qualitative similarity of the experimentally recorded trajectories in Fig. 2 to their numerically generated

[1]Note that the distribution of the counting rate is not identical with the distribution P_{st} given by the stationary solution of the Fokker-Planck equation belonging to the Langevin equation (16). The difference results from the nonlinear transformation of infinitesimal area elements from Cartesian to polar coordinates,

$$\int\int dv_x dv_y=\int\int v\,dv\,d\varphi=2\pi\int v\,dv, \tag{24}$$

which has to be taken into account for the calculation of P_{st}.

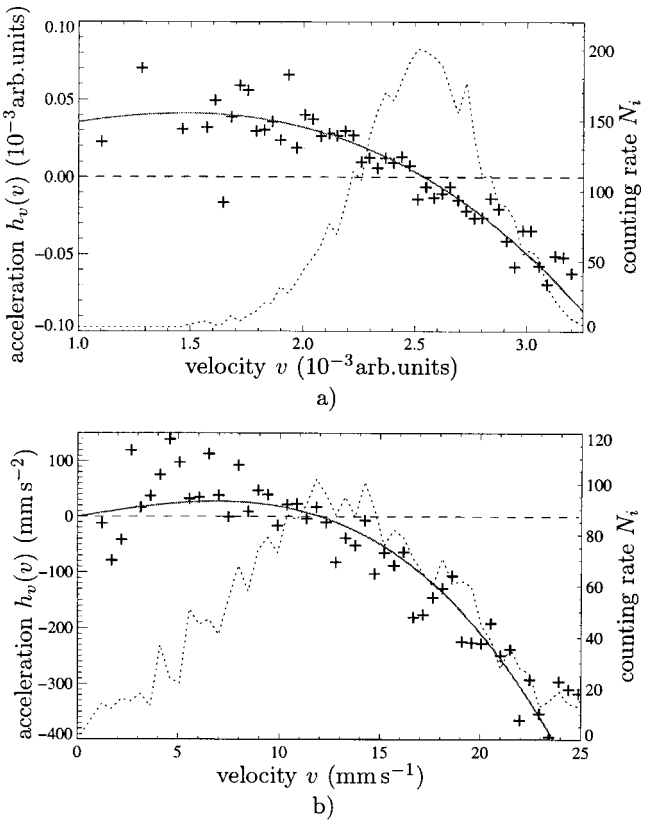

FIG. 5. Results of the stochastic data analysis technique for the trajectories shown in Figs. 2(a) and 4(a). Crosses mark the deterministic part $h_v(v)$ of the dynamics for each bin as a result of the data analysis technique, and dotted curves correspond to the frequency polygons of the corresponding counting rates N_i. (a) Analysis of the numerically calculated trajectory of Fig. 4(a) with bin width $\Delta v = 3.6 \times 10^{-5}$. The gray curve shows the theoretical deterministic dynamics given by Eq. (20) for the corresponding parameters. The intersection point of the theoretical curve with the abscissa is the intrinsic velocity v_0 [see Eq. (5)]. (b) Analysis of the experimentally observed trajectory depicted in Fig. 2(a) with bin width $\Delta v = 0.5$ mm s^{-1}. Here the gray line is a nonlinear fit according to Eq. (6) for bins with counting rates $N_i > 10$. The filament moves with an intrinsic velocity $v_0 \approx 11$ mm s^{-1}.

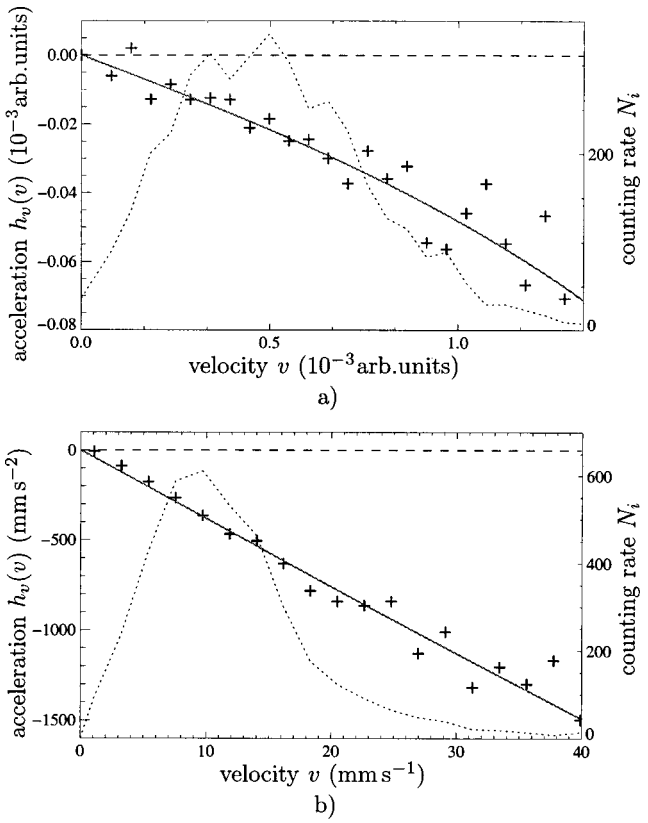

FIG. 6. Results of the data analysis technique for the trajectories shown in Figs. 2(b) and 4(b). (a) Calculated (crosses) and theoretical (gray curve) deterministic dynamics for the numerically calculated trajectory depicted in Fig. 4(b). The data analysis algorithm has been run with bin width $\Delta v = 5.3 \times 10^{-5}$. (b) Calculated (crosses) and fitted (gray curve) deterministic dynamics of the experimentally observed DS propagating as depicted in Fig. 2(b) with bin width $\Delta v = 2$ mm s^{-1}.

counterparts in Fig. 4, the corresponding data series are considered as a good starting point for the experimental application of the data analysis that was described in Sec. III.

In Fig. 2(a), the luminance distribution of the gas discharge was recorded for an overall time of 62 s. The result of applying the data analysis technique to the corresponding time series with 50 bins of width $\Delta v = 0.5$ mm s^{-1} is shown in Fig. 5(b). Here, as in Fig. 5(a), the dotted curve represents the frequency polygon of the counting rate and the black crosses represent the calculated acceleration due to the intrinsic dynamics of the DS. For the reliable bins ($N_i > 10$), motivated by Eq. (6) a cubic curve, which is depicted as the gray line, has been fitted to the result of the data analysis with the least squares method. The intersection point of this curve with the abscissa at $v_0 = 11$ mm s^{-1} corresponds to the intrinsic velocity of the experimentally observed DS for the chosen parameters. As in the case of the simulated particle dynamics in Fig. 5(a), the frequency polygon has its maximum close to this point, confirming that the DS moves with its intrinsic velocity most of the time. In the absence of noise and for an ideal homogeneous and unbounded system, the experimentally observed DS would travel with finite constant velocity v_0 for infinite time.

The trajectories depicted in Fig. 2(b) were recorded for 72 s. In view of the apparent difference of Fig. 2(a) from Fig. 2(b), a different result of the analysis may be expected. This is confirmed when using the method discussed with 20 bins of width $\Delta v = 2$ mm s^{-1}. The result is depicted in Fig. 6(b), where it can be seen that the acceleration of the DS is almost proportional to the velocity with a negative proportionality constant. This means that, in contrast to the intrinsically moving DS in Fig. 2(a), the motion is purely damped, in the depicted case with a damping constant of $\gamma = 37.6 \pm 1.5$ s^{-1} computed from a linear least squares fit. The DS has no intrinsic deterministic velocity at all and would remain stationary without the driving influence of noise. This case cor-

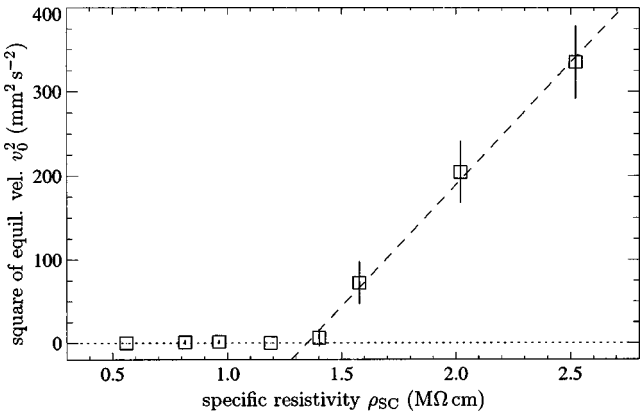

FIG. 7. Results of the stochastic data analysis for intrinsic velocity v_0 of the experimentally observed DSs as a function of the specific resistivity of the semiconductor. For every value of the resistivity, the velocity v_0 was determined by a polynomial fit. Parameters: $U_0=3700$ V, $R_0=10$ MΩ, $p=286$ hPa, $d=750$ μm, all other parameters as in Fig. 2(a). The global current was $I=107$ μA.

responds to a classical Ornstein-Uhlenbeck process.[2] Note that the Ornstein-Uhlenbeck process is also approximately realized in the theoretical model [Fig. 6(a)].

The results depicted in Fig. 5 and 6 provide an explanation for the qualitative similarities of the experimentally observed and numerically calculated trajectories: although in the derivation of Eq. (16) only symmetry arguments were used, the deterministic part of the dynamics extracted from the experimental data can be represented by the theoretically derived reduced dynamics in a satisfying way. Further investigations for other points in parameter space in which only one filament is present at a given time have confirmed that the deterministic part of the dynamics can always be classified according to the two qualitatively different cases presented above, and that the functional form of the drift function can be represented by the theoretically predicted third-order polynomial. This observation gives rise to the question whether a drift bifurcation, i.e., a transition between the two states, can be detected in the experiment and which experimental parameter should be used as the control parameter.

B. The drift bifurcation

In a systematic investigation, it turned out that a drift bifurcation can actually be found in the experiment by using the specific resistivity ρ_{SC} of the semiconductor as the control parameter. Keeping all other parameters fixed, the specific resistivity was varied and the corresponding intrinsic velocity v_0 was extracted from the recorded trajectories using a third-order polynomial fit. In order to visualize the dependence of the measured intrinsic velocity on the control parameter ρ_{SC}, the square of v_0 has been plotted as a function of ρ_{SC} (Fig. 7), revealing a supercritical bifurcation of pitchfork shape.

These findings are reflected in the three-component reaction-diffusion system (1) and its reduced dynamics (3) and (4), predicting a pitchforklike bifurcation when varying τ [see Eq. (6) and the corresponding scaling law (5) for the velocity of the DS] [31]. Due to the correct qualitative predictions given by the model equations for many experimental observations, it is tempting to relate the parameter τ of the theoretical model to the parameter ρ_{SC} of the gas-discharge device. In fact, it can be seen from the original derivation of the reaction-diffusion system using equivalent circuit considerations [23,38] that τ increases monotonically with ρ_{SC}. However, ρ_{SC} also enters into other parameters of Eq. (1). This means that, while the transition from a region of stationary DSs to a region of intrinsically moving DSs described by Eq. (5) takes place along a line parallel to the τ axis, the transition due to a variation of ρ_{SC} takes place along a different path in the model parameter space. Despite this fact, a linear dependance of v_0^2 on the bifurcation parameter is observed in both cases, as the qualitative properties of the bifurcation are independent of the exact path in the generic case when close to the bifurcation point.

VI. SUMMARY AND OUTLOOK

In the present work we have investigated the dynamics of electrical current filaments in a quasi-two-dimensional dc gas-discharge system with high Ohmic barrier. We refer to these filaments as dissipative solitons. As the dynamics of the experimentally observed DSs is strongly influenced by noise, a data-driven stochastic time series analysis technique has been developed to separate the deterministic from the stochastic part of the dynamics. The efficiency of the analysis technique was proved using a set of ordinary differential equations which provide a qualitative description of the propagation of DSs in the mentioned gas-discharge system. To these deterministic equations, uncorrelated Gaussian noise was added artificially. Using this technique, the correct deterministic part of the dynamics of the DSs could be reconstructed.

The analysis of the dynamics of the experimentally observed DSs has demonstrated that their dynamic behavior can be separated into two qualitatively different regimes. On one hand, one deals with noise-driven DSs, which would remain stationary in the absence of stochastic fluctuations. In this case, the dynamics corresponds to that of a classical Brownian particle. On the other hand, we observe intrinsically moving DSs that travel with a dynamically stabilized finite velocity. The DSs in this regime are also referred to as *active Brownian particles* [59]. A transition between these two regimes was detected by choosing the specific resistivity of the semiconductor as the control parameter. The corresponding experimentally obtained drift bifurcation is in good agreement with the prediction of a supercritical pitchforklike bifurcation resulting from modeling of the experimental gas-discharge system using a set of reaction-diffusion equations.

[2]This is confirmed through the calculation of P_{st}, the stationary solution of the corresponding Fokker-Planck equation, from the counting rate distribution, as P_{st} is a Gaussian distribution with a central second moment of 19.1 mm s^{-1}.

As a rather wide class of dynamic systems can be described by Langevin equations of the form (7), this stochastic data analysis technique will certainly find many other areas of application.

ACKNOWLEDGMENTS

We gratefully acknowledge support of this work by the Deutsche Forschungsgemeinschaft. Furthermore, the authors would like to thank A. S. Moskalenko and J. Berkemeier for fruitful discussions and St. Flothkötter for developing the programs that have been used to extract the trajectories of the DSs from the recorded luminance distributions of the gas discharge.

APPENDIX: MATHEMATICAL PROOF

The goal of the appendix is to prove the validity of Eqs. (18) and (19). A direct transformation of Eq. (15) into polar coordinates using the chain rule yields Eq. (17) with multiplicative noise. To find a stochastically equivalent equation with additive noise, one has to set up the corresponding Fokker-Planck equation. Using the notation of Eq. (7), the drift coefficient $D_i^{(1)}$ with $i \in \{v,\varphi\}$ for the velocity component takes the form

$$D_v^{(1)} = h_v + g_{kj}\frac{\partial}{\partial q_k} g_{ij} \overset{(17)}{=} h_v + g_{\varphi v}\frac{\partial}{\partial \varphi} g_{vv} + g_{\varphi\varphi}\frac{\partial}{\partial \varphi} g_{v\varphi} = h_v + \frac{R^2}{v}. \tag{A1}$$

For the diffusion coefficient D_{ik} with $i,k \in \{v,\varphi\}$, one finds for $i,k=v$ (see also [56], Sec. 12.1.2)

$$D_{vv}^{(2)} = R. \tag{A2}$$

This yields the Langevin equation

$$\dot{v}(t) = h_v(v) + \frac{R^2}{v} + R\Gamma_v(t), \tag{A3}$$

with the effective force

$$h_{eff}(v) = h_v(v) + \frac{R^2}{v} \tag{A4}$$

and $\Gamma_v(t)$ satisfying Eqs. (8) and (9). Applying the data analysis technique discussed in Sec. IV yields the first Kramers-Moyal (KM) coefficient of Eq. (A3):

$$D_v^{(1)}(v) = \lim_{\Delta t\to 0}\frac{1}{\Delta t}\langle v'(t+\Delta t) - v'(t)\rangle\big|_{v'(t)=v}. \tag{A5}$$

The second KM coefficient of Eq. (A3) can be determined by

$$D_v^{(2)}(v) = R^2 = \frac{1}{2}\lim_{\Delta t\to 0}\frac{1}{\Delta t}\langle [v'(t+\Delta t) - v'(t)]^2\rangle\big|_{v'(t)=v}, \tag{A6}$$

where $v'(t)$ is a solution of Eq. (A3). Calculating R^2 is also possible by determining the second KM coefficients $D_{ik}^{(2)}$ with $i,k=x,y$ from Eq. (16) using

$$D_{i,k}^{(2)}(\boldsymbol{v}) = \frac{1}{2}\lim_{\Delta t\to 0}\frac{1}{\Delta t}\langle [v_i'(t+\Delta t) - v_i'(t)] \times [v_k'(t+\Delta t) - v_k'(t)]\rangle\big|_{\boldsymbol{v}'(t)=\boldsymbol{v}} \tag{A7}$$

if $\boldsymbol{v}'(t)$ is a solution of Eq. (16). With a noise amplitude independent of $\boldsymbol{v}$, Eq. (A7) can be transformed into

$$R^2\delta_{ik} = \frac{1}{2}\lim_{\Delta t\to 0}\frac{1}{\Delta t}\langle [v_i'(t+\Delta t) - v_i'(t)] \times [v_k'(t+\Delta t) - v_k'(t)]\rangle\big|_{|\boldsymbol{v}'(t)|=|\boldsymbol{v}|}. \tag{A8}$$

In order to prove Eq. (19) one adds Eq. (A8) with $i,k=x$ and $i,k=y$, to find

$$2R^2 = \frac{1}{2}\lim_{\Delta t\to 0}\frac{1}{\Delta t}\langle v'^2(t+\Delta t) + v'^2(t) - 2\boldsymbol{v}'(t+\Delta t)\boldsymbol{v}'(t)\rangle\big|_{v'(t)=v}. \tag{A9}$$

Substracting Eq. (A6) from Eq. (A9) yields

$$R^2 = \lim_{\Delta t\to 0}\frac{1}{\Delta t}\langle v'(t+\Delta t)v'(t) - \boldsymbol{v}'(t+\Delta t)\boldsymbol{v}'(t)\rangle\big|_{v'(t)=v}. \tag{A10}$$

In order to calculate $h_v(v)$ without determining R from the experimental data, one takes advantage of

$$h_v(v) = \lim_{\Delta t\to 0}\frac{1}{\Delta t}\langle v'(t+\Delta t) - v'(t)\rangle\big|_{v'(t)=v} - \frac{R^2}{v} \tag{A11}$$

[see Eq. (A5)] and inserts Eq. (A10):

$$h_v(v) = \lim_{\Delta t\to 0}\frac{1}{\Delta t}\langle v'(t+\Delta t) - v'(t)\rangle\big|_{v'(t)=v} - \frac{1}{v}\lim_{\Delta t\to 0}\frac{1}{\Delta t}\langle v'(t+\Delta t)v'(t) - \boldsymbol{v}'(t+\Delta t)\cdot\boldsymbol{v}'(t)\rangle\Big|_{v'(t)=v}$$

$$= \lim_{\Delta t\to 0}\frac{1}{\Delta t}\langle v'(t+\Delta t) - v'(t)\rangle\big|_{v'(t)=v} - \lim_{\Delta t\to 0}\frac{1}{\Delta t}\left\langle \frac{v'(t+\Delta t)v'(t) - \boldsymbol{v}'(t+\Delta t)\cdot\boldsymbol{v}'(t)}{v}\right\rangle\Big|_{v'(t)=v}$$

$$= \lim_{\Delta t\to 0}\frac{1}{\Delta t}\langle v'(t+\Delta t)-v'(t)\rangle|_{v'(t)=v} - \lim_{\Delta t\to 0}\frac{1}{\Delta t}\left\langle \frac{v'(t+\Delta t)v'(t)-\boldsymbol{v}'(t+\Delta t)\cdot\boldsymbol{v}'(t)}{v'(t)}\right\rangle\Bigg|_{v'(t)=v}$$

$$= \lim_{\Delta t\to 0}\frac{1}{\Delta t}\langle v'(t+\Delta t)-v'(t)\rangle|_{v'(t)=v} - \lim_{\Delta t\to 0}\frac{1}{\Delta t}\left\langle v'(t+\Delta t)-\boldsymbol{v}'(t+\Delta t)\cdot\frac{\boldsymbol{v}'(t)}{v'(t)}\right\rangle\Bigg|_{v'(t)=v}$$

$$= \lim_{\Delta t\to 0}\frac{1}{\Delta t}\left\langle \boldsymbol{v}'(t+\Delta t)\cdot\frac{\boldsymbol{v}'(t)}{v'(t)}-v'(t)\right\rangle\Bigg|_{v'(t)=v}. \tag{A12}$$

This corresponds to Eq. (19). Note that this ''projection method'' gives a solution to the problem addressed in [56], Sec. 12.1.2, of how to determine h_v without explicitly computing the fluctuation strength R.

[1] R. Rajaraman, *Solitons and Instantons: An Introduction to Solitons and Instantons in Quantum Field Theory* (North-Holland, Amsterdam, 1982).

[2] M. Remoissenet, *Waves Called Solitons: Concepts and Experiments*, 3rd ed. (Springer, Berlin, 1999).

[3] C.I. Christov and M.G. Velarde, Physica D **86**, 323 (1995).

[4] B.S. Kerner and V.V. Osipov, *Autosolitons: A New Approach to Problems of Self-Organization and Turbulence*, Vol. 61 of *Fundamental Theories of Physics* (Kluwer Academic, Dordrecht, 1994).

[5] M. Bode and H.-G. Purwins, Physica D **86**, 53 (1995).

[6] A.L. Hodgkin and A.F. Huxley, J. Physiol. (London) **117**, 500 (1952).

[7] Q. Ouyang, V. Castets, J. Boissonade, J.C. Roux, P.D. Kepper, and H.L. Swinney, J. Chem. Phys. **95**, 351 (1991).

[8] H.H. Rotermund, S. Jakubith, A. von Oertzen, and G. Ertl, Phys. Rev. Lett. **66**, 3083 (1991).

[9] K.-J. Lee, W.D. McCormick, J.E. Pearson, and H.L. Swinney, Nature (London) **369**, 215 (1994).

[10] F.T. Arecchi, S. Boccaletti, and P. Ramazza, Phys. Rep. **328**, 1 (1999).

[11] T. Ackemann and W. Lange, Appl. Phys. B: Lasers Opt. **72**, 21 (2001).

[12] V.V. Bel'kov, J. Hirschinger, V. Novák, F. Niedernostheide, S.D. Ganichev, and W. Prettl, Nature (London) **397**, 398 (1999).

[13] K. Aoki, *Nonlinear Dynamics and Chaos in Semiconductors* (Institute of Physics Publishing, Bristol, 2001).

[14] E. Schöll, *Nonlinear Spatio-Temporal Dynamics and Chaos in Semiconductors*, Vol. 10 of *Cambridge Nonlinear Science Series* (Cambridge University Press, Cambridge, England, 2001).

[15] E. Schöll, F. Niedernostheide, J. Parisi, W. Prettl, and H.-G. Purwins, in *Evolution of Spontaneous Structures in Dissipative Continuous Systems*, edited by F. H. Busse and S. C. Müller (Wissenschaft und Technik Verlag, Berlin, 1998), pp. 446–494.

[16] F.-J. Niedernostheide, M. Arps, R. Dohmen, H. Willebrand, and H.-G. Purwins, Phys. Status Solidi B **172**, 249 (1992).

[17] Y.A. Astrov and H.-G. Purwins, Phys. Lett. A **283**, 349 (2001).

[18] Y.A. Astrov, L.M. Portsel, S.P. Teperick, H. Willebrand, and H.-G. Purwins, J. Appl. Phys. **74**, 2159 (1993).

[19] I. Brauer, dissertation, Institut für Angewandte Physik, Westfälische Wilhelms-Universität, Münster, 2000.

[20] H.-G. Purwins, Y. Astrov, and I. Brauer, in *The 5th Experimental Chaos Conference, Orlando, FL, 1999*, edited by M. Ding, W. L. Ditto, L. M. Pecora, and M. L. Spano (World Scientific, Singapore, 2001), pp. 3–13.

[21] H.-G. Purwins, Y. A. Astrov, I. Brauer, and M. Bode, in *RIMS Project 2000: Reaction-Diffusion Systems: Theory and Application. Interfaces, Pulses and Waves in Nonlinear Dissipative Systems* (Research Institute for Mathematical Sciences, Kyoto University, Kyoto, Japan, 2001), pp. 1–8.

[22] C. Radehaus, K. Kardell, H. Baumann, D. Jäger, and H.-G. Purwins, Z. Phys. B: Condens. Matter **65**, 515 (1987).

[23] H.-G. Purwins, C. Radehaus, and J. Berkemeier, Z. Naturforsch., A: Phys. Sci. **43**, 17 (1988).

[24] L.M. Portsel, Y.A. Astrov, I. Reimann, E. Ammelt, and H.-G. Purwins, J. Appl. Phys. **85**, 3960 (1999).

[25] Y.A. Astrov and Y.A. Logvin, Phys. Rev. Lett. **79**, 2983 (1997).

[26] M. Bode, A.W. Liehr, C.P. Schenk, and H.-G. Purwins, Physica D **161**, 45 (2002).

[27] H. Meinhardt, *Models of Biological Pattern Formation* (Academic Press, London, 1982).

[28] J. D. Murray, *Mathematical Biology* (Springer, Berlin, 1993).

[29] M.C. Cross and P.C. Hohenberg, Rev. Mod. Phys. **65**, 851 (1993).

[30] M. Bode, Physica D **106**, 270 (1997).

[31] M. Or-Guil, M. Bode, C.P. Schenk, and H.-G. Purwins, Phys. Rev. E **57**, 6432 (1998).

[32] C.P. Schenk, P. Schütz, M. Bode, and H.-G. Purwins, Phys. Rev. E **57**, 6480 (1998).

[33] S. Siegert, R. Friedrich, and J. Peinke, Phys. Lett. A **243**, 275 (1998).

[34] R. Friedrich, S. Siegert, S. Lück, M. Siefert, M. Lindemann, J. Raethjen, G. Deutschl, and G. Pfister, Phys. Lett. A **271**, 217 (2000).

[35] S. Matern, V.M. Marchenko, Y.A. Astrov, L.M. Portsel, and H.-G. Purwins, Proc. SPIE **4669**, 13 (2002).

[36] C. Strümpel, H.-G. Purwins, and Y.A. Astrov, Phys. Rev. E **63**, 026409/1 (2001).

[37] V.M. Marchenko, S. Matern, Y.A. Astrov, L.M. Portsel, and H.-G. Purwins, Proc. SPIE **4669**, 1 (2002).

[38] H.-G. Purwins, G. Klempt, and J. Berkemeier, Festkoerperprobleme **27**, 27 (1987).
[39] C. Radehaus, T. Dirksmeyer, H. Willebrand, and H.-G. Purwins, Phys. Lett. A **125**, 92 (1987).
[40] C.P. Schenk, M. Or-Guil, M. Bode, and H.-G. Purwins, Phys. Rev. Lett. **78**, 3781 (1997).
[41] E. Ammelt, Y.A. Astrov, and H.-G. Purwins, Phys. Rev. E **58**, 7109 (1998).
[42] A.M. Turing, Philos. Trans. R. Soc. London, Ser. B **237**, 37 (1952).
[43] A.W. Liehr, M. Bode, and H.-G. Purwins, in *High Performance Computing in Science and Engineering 2000: Transactions of the High Performance Computing Center, Stuttgart (HLRS) 2000*, edited by E. Krause and W. Jäger (Springer, Berlin, 2001), pp. 425–439.
[44] H.-G. Purwins, C. Radehaus, T. Dirksmeyer, R. Dohmen, R. Schmeling, and H. Willebrand, Phys. Lett. A **136**, 480 (1989).
[45] C. Radehaus, H. Willebrand, R. Dohmen, F.-J. Niedernostheide, G. Bengel, and H.-G. Purwins, Phys. Rev. A **45**, 2546 (1992).
[46] T. Ohta, Physica D **151**, 61 (2001).
[47] K. Krischer and A. Mikhailov, Phys. Rev. Lett. **73**, 3165 (1994).
[48] L.M. Pismen, Phys. Rev. Lett. **86**, 548 (2001).
[49] C.P. Schenk, A.W. Liehr, M. Bode, and H.-G. Purwins, in *High Performance Computing in Science and Engineering '99: Transactions of the High Performance Computing Center, Stuttgart 1999*, edited by E. Krause and W. Jäger (Springer, Berlin, 2000), pp. 354–364.
[50] R.S. Islamov, Phys. Rev. E **64**, 046405 (2001).
[51] I. Brauer, C. Punset, H.-G. Purwins, and J.P. Boeuf, J. Appl. Phys. **85**, 7569 (1999).
[52] A.S. Moskalenko, A.W. Liehr, and H.-G. Purwins (unpublished).
[53] R. Friedrich, Z. Phys. B: Condens. Matter **90**, 373 (1993).
[54] H. Haken, *Synergetics, An Introduction*, 3rd ed. (Springer, Berlin, New York, 1983).
[55] A. Kolmogorov, Math. Ann. **104**, 415 (1931).
[56] H. Risken, *The Fokker-Planck-Equation: Methods of Solution and Applications* (Springer, Berlin, 1996).
[57] R.L. Stratonovich, *Conditional Markov Processes and Their Application to the Theory of Optimal Control* (Elsevier, New York, 1968).
[58] A.W. Liehr, A.S. Moskalenko, Y.A. Astrov, M. Bode, and H.-G. Purwins (unpublished).
[59] U. Erdmann, W. Ebeling, L. Schimansky-Geier, and F. Schweitzer, Eur. Phys. J. B **15**, 105 (2000).